CANCER

Drugging the catalytically inactive state of RET kinase in RET-rearranged tumors

Dennis Plenker,[1,2]* Maximilian Riedel,[1,2]* Johannes Brägelmann,[1,2] Marcel A. Dammert,[1,2] Rakhee Chauhan,[3] Phillip P. Knowles,[3] Carina Lorenz,[1,2] Marina Keul,[4] Mike Bührmann,[4] Oliver Pagel,[5] Verena Tischler,[2] Andreas H. Scheel,[6] Daniel Schütte,[2] Yanrui Song,[7] Justina Stark,[4] Florian Mrugalla,[4] Yannic Alber,[4] André Richters,[4] Julian Engel,[4] Frauke Leenders,[8] Johannes M. Heuckmann,[8] Jürgen Wolf,[9] Joachim Diebold,[10] Georg Pall,[11] Martin Peifer,[2] Maarten Aerts,[12,13] Kris Gevaert,[12,13] René P. Zahedi,[5] Reinhard Buettner,[6] Kevan M. Shokat,[14] Neil Q. McDonald,[3,15] Stefan M. Kast,[4] Oliver Gautschi,[10†] Roman K. Thomas,[2,9,16†] Martin L. Sos[1,2†‡]

Oncogenic fusion events have been identified in a broad range of tumors. Among them, *RET* rearrangements represent distinct and potentially druggable targets that are recurrently found in lung adenocarcinomas. We provide further evidence that current anti-RET drugs may not be potent enough to induce durable responses in such tumors. We report that potent inhibitors, such as AD80 or ponatinib, that stably bind in the DFG-out conformation of RET may overcome these limitations and selectively kill *RET*-rearranged tumors. Using chemical genomics in conjunction with phosphoproteomic analyses in *RET*-rearranged cells, we identify the CCDC6-RET^{I788N} mutation and drug-induced mitogen-activated protein kinase pathway reactivation as possible mechanisms by which tumors may escape the activity of RET inhibitors. Our data provide mechanistic insight into the druggability of RET kinase fusions that may be of help for the development of effective therapies targeting such tumors.

INTRODUCTION

Targeted inhibition of oncogenic driver mutations with small molecules is a cornerstone of precision cancer medicine. *RET* rearrangements have been identified in a broad range of tumors, including 1 to 2% of lung adenocarcinomas, and their discovery sparked the hope for an effective treatment option in these patients (*1*–*3*). However, when compared to other oncogenic "driver" alterations, such as rearranged anaplastic lymphoma kinase (ALK), rearranged RET seems to be a difficult target, and to date, no drug has been successfully established for the treatment of these tumors (*4*–*6*). Recent clinical data suggest that overall response rates in patients treated with currently available RET-targeted drugs are rather limited and range between 18 and 53% (*7*–*10*). Improved selection of patients based on deep sequencing of individual tumors may help increase these response rates, but still progression-free survival seems to be very limited (*7*, *8*, *10*, *11*). These observations are particularly surprising from a chemical point of view because a broad spectrum of kinase inhibitors is known to bind to RET and to inhibit its kinase activity in vitro (*6*, *12*). On the basis of these observations, we sought to characterize rearranged RET in independent cancer models to identify potent RET inhibitors with high selectivity and optimal biochemical profile to target *RET*-rearranged tumors.

RESULTS

Kinase inhibitor AD80 shows extraordinary activity in *RET*-rearranged cancer models

Because clinical experience with RET-targeted drugs in lung cancer patients is rather disappointing, we sought to test a series of clinically and preclinically available drugs with anti-RET activity in Ba/F3 cells engineered to express either *KIF5B-RET* or *CCDC6-RET* (*1*, *2*, *12*, *13*). In these experiments, AD80 and ponatinib exhibited 100- to 1000-fold higher cytotoxicity compared to all other tested drugs in RET-dependent, but not interleukin-3–supplemented, Ba/F3 cells (Fig. 1A and fig. S1, A and B). In line with these results, AD80, but not cabozantinib or vandetanib, prevented the phosphorylation of RET as well as of extracellular signal–regulated kinase (ERK), AKT, and S6K at low nanomolar concentrations in kinesin family member 5B (KIF5B)–RET–expressing Ba/F3 cells (Fig. 1B and table S1). These data are in line with our own retrospective analysis where out of four patients with *RET*-rearranged tumors, we observed only one partial response in a patient receiving vandetanib (P2) as first-line treatment (fig. S1, C to E, and table S2, A and B) (*9*). Sequencing of rebiopsy samples did not reveal candidate drug resistance mutations, suggesting that the target had been insufficiently inhibited (table S2C).

To validate the efficacy of AD80 and ponatinib in an alternative model, we induced *KIF5B-RET* rearrangements (*KIF5B* exon 15; *RET* exon 12) in NIH-3T3 cells using clustered regularly interspaced short

[1]Molecular Pathology, Institute of Pathology, Center of Integrated Oncology, University Hospital Cologne, 50937 Cologne, Germany. [2]Department of Translational Genomics, Center of Integrated Oncology Cologne–Bonn, Medical Faculty, University of Cologne, 50931 Cologne, Germany. [3]Structural Biology Laboratory, Francis Crick Institute, 44 Lincoln's Inn Fields, London WC2A 3LY, UK. [4]Faculty of Chemistry and Chemical Biology, TU Dortmund University, 44227 Dortmund, Germany. [5]Leibniz-Institut für Analytische Wissenschaften–ISAS–e.V., Dortmund, Germany. [6]Institute of Pathology, Center of Integrated Oncology, University Hospital Cologne, 50937 Cologne, Germany. [7]Crown BioScience, Inc., 3375 Scott Blvd, Suite 108, Santa Clara, CA 95054, USA. [8]NEO New Oncology GmbH, 51105 Cologne, Germany. [9]Department of Internal Medicine, Center for Integrated Oncology Köln Bonn, University Hospital Cologne, Cologne, 50931 Cologne, Germany. [10]Cancer Center, Lucerne Cantonal Hospital, 6000 Lucerne, Switzerland. [11]Department of Internal Medicine 5, University Hospital Innsbruck, Haematology/Oncology, Anichstraße 35, 6020 Innsbruck, Austria. [12]VIB-UGent Center for Medical Biotechnology, VIB, B-9000 Ghent, Belgium. [13]Department of Biochemistry, Ghent University, B-9000 Ghent, Belgium. [14]Department of Cellular and Molecular Pharmacology, Howard Hughes Medical Institute, University of California, San Francisco, San Francisco, CA 94158, USA. [15]Institute of Structural and Molecular Biology, Department of Biological Sciences, Birkbeck College, Malet Street, London WC1E 7HX, UK. [16]German Cancer Consortium (DKTK), partner site Heidelberg, and German Cancer Research Center (DKFZ), Heidelberg, Germany.
*These authors contributed equally to this work.
†These authors contributed equally to this work.
‡Corresponding author. Email: martin.sos@uni-koeln.de

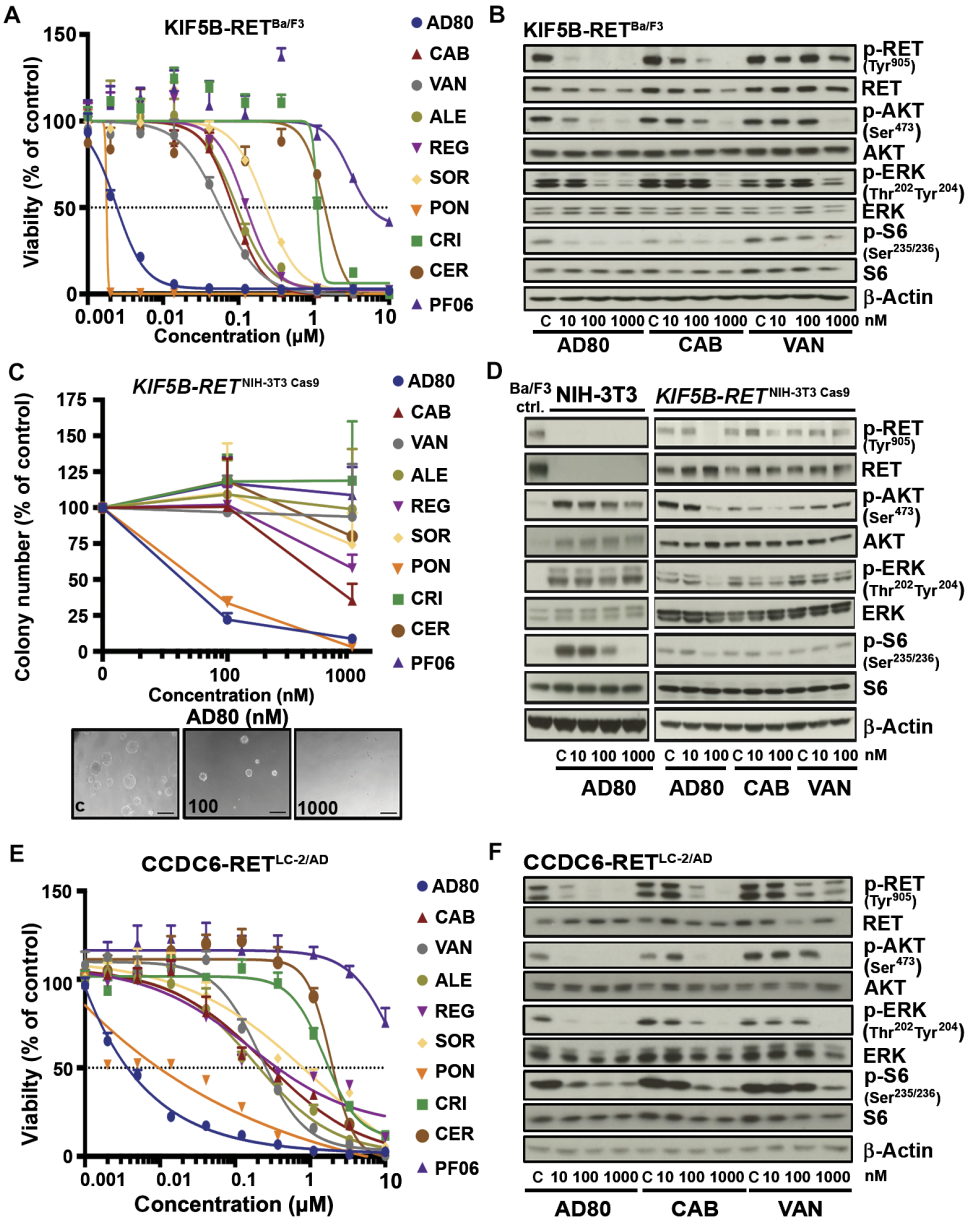

Fig. 1. Cellular profiling of RET inhibitors identifies AD80 and ponatinib as potent compounds. (**A**) Dose-response curves (72 hours) for AD80, cabozantinib (CAB), vandetanib (VAN), alectinib (ALE), regorafenib (REG), sorafenib (SOR), ponatinib (PON), crizotinib (CRI), ceritinib (CER), or PF06463922 (PF06) in KIF5B-RET–expressing Ba/F3 cells ($n = 3$ technical replicates). (**B**) Immunoblotting results of *KIF5B-RET*–rearranged Ba/F3 cells after treatment (4 hours). C, control. (**C**) Relative mean colony number of NIH-3T3 cells engineered with *KIF5B-RET* fusion by CRISPR/Cas9 was assessed in soft agar assays after 7 days under treatment. Representative images of colonies under AD80 treatment are displayed in the lower panel. Scale bars, 100 μm ($n = 3$) (**D**) Immunoblotting of CRISPR/Cas9-engineered, *KIF5B-RET*–rearranged NIH-3T3 cells treated with AD80, cabozantinib, or vandetanib (4 hours). *KIF5B-RET* expressing Ba/F3 cells (Ba/F3 ctrl.) serve as control for RET signaling ($n = 3$) (**E**) Dose-response curves (72 hours) for different inhibitors in LC-2/AD cells. (**F**) Immunoblotting was performed in LC-2/AD cells treated with AD80, cabozantinib, or vandetanib (4 hours).

palindromic repeats (CRISPR)/Cas9–meditated genome editing. We confirmed their anchorage-independent growth, increased proliferation rate, and high sensitivity to AD80 and ponatinib (Fig. 1C and fig. S2, A to C) (*14*). Again, treatment with AD80, but not cabozantinib or vandetanib, led to inhibition of phosphorylated RET (phospho-RET) and of downstream effectors of RET signaling at low nanomolar concentrations (Fig. 1D). AD80 led to dephosphorylation of S6 also in parental NIH-3T3 cells and Ba/F3$^{myr\text{-}AKT}$ control cells, suggesting that S6 may represent an off-target at micromolar concentrations (Fig. 1D and fig. S2D) (*13*).

To further substantiate our results, we next tested our panel of RET inhibitors in the *CCDC6-RET* rearranged lung adenocarcinoma cell line LC-2/AD (*15*). We observed similar activity profiles with AD80 followed by ponatinib as the most potent inhibitors compared to all other tested drugs in terms of cytotoxicity at low nanomolar concentrations (Fig. 1E) and inhibition of phospho-RET and other downstream signaling molecules (Fig. 1F). Overall, our data suggest that in *RET*-rearranged cells, AD80 and ponatinib are 100- to 1000-fold more effective against RET and its downstream signaling than any other clinically tested anti-RET drug.

AD80 and ponatinib effectively inhibit RET kinase in DFG-out conformation

We benchmarked the genotype-specific activity of AD80 and ponatinib against well-described kinase inhibitors, such as erlotinib, BGJ398, vandetanib, cabozantinib, regorafenib, alectinib, and ceritinib, in a panel of 18 cancer cell lines driven by known oncogenic lesions, such as mutant epidermal growth factor receptor (EGFR) or rearranged ALK, including two *RET*-rearranged cell lines (LC-2/AD and TPC-1) (fig. S3A) (*6*, *12*, *16*). Again, we identified AD80 and ponatinib as the most effective drugs and, through the calculation of median on-target versus off-target ratios, also as the most specific drugs in *RET* fusion–positive cells (fig. S3B and table S3).

To further characterize intracellular signaling induced by an RET inhibitor, such as AD80, we performed mass spectrometry–based phosphoproteomic analyses of LC-2/AD cells treated with 10 or 100 nM AD80. In AD80-treated cells, we observed a significant decrease of RET^{Y900} phosphorylation with $\log_2$-fold changes of −1.07 ($P = 0.009$; 10 nM AD80) and −2.11 ($P = 0.0002$; 100 nM AD80), respectively (Fig. 2A). Among all phosphopeptides quantified under control, 10 nM, and 100 nM conditions ($n = 11912$), the abundance of RET^{Y900} was among the most decreased phosphopeptides (control versus 100 nM AD80; $P = 0.00024$) and the most decreased receptor tyrosine kinases (fig. S3C). These results highlight that in these cells, RET is the primary target of AD80.

On the basis of these observations, we speculated that activation of RET-independent signaling pathways should largely abrogate the

cytotoxic effects of AD80. To this end, we supplemented LC-2/AD cells with exogenous receptor ligands and found that the activity of AD80 was significantly reduced ($P \leq 0.05$) through the addition of EGF, hepatocyte growth factor, and neuregulin 1, indicating that RET is the primary cellular target in *RET*-rearranged LC-2/AD cells (fig. S4A).

To further characterize the high potency of AD80 and ponatinib against RET kinase fusions, we expressed and purified different truncated versions of the RET core kinase and juxtamembrane-kinase domain, as well as truncated forms of both coiled-coil domain containing 6 (CCDC6) (ΔCCDC6-KD) and KIF5B (ΔKIF5B-KD) kinase domain fusions (fig. S4, B and C) (*17*). We used these different RET fusion kinase domain constructs to determine the extent to which binding of a given compound has an effect on protein thermal stability, as measured by the melting temperature (T_m). The difference in melting temperature with and without drug (ΔT_m) extrapolates the potency of the individual drugs against the respective constructs (*17*). To our surprise, we found that treatment with the type I inhibitors sunitinib or vandetanib resulted in a ΔT_m of only 1° to 4°C, whereas the type II inhibitors sorafenib, ponatinib, or AD80 increased the ΔT_m of up to 10° to 18°C (Fig. 2B and fig. S4, D to H). We observed the strongest effects in ΔKIF5B-KD and ΔCCDC6-KD constructs treated with AD80 and core KD with ponatinib (Fig. 2B, fig. S4D, and table S4). Such a shift for inhibitors that stabilize the catalytically inactive conformation of RET kinase, in which the DFG motif is flipped out (DFG-out) relative to its conformation in the active state (DFG-in), does not correlate with the differential in vitro kinase activity observed for sorafenib and other RET inhibitors (table S5) (*6*, *18*).

To further characterize the relevance of a DFG-out conformation for the activity of RET inhibitors, we performed structural analyses. We used homology modeling based on a vascular EGFR (VEGFR) kinase [Protein Data Bank (PDB) code 2OH4 (*19*)] in the DFG-out complex similar to a previously published methodology (*20*), followed by extensive molecular dynamics (MD) simulation refinement. We observed that the root mean square deviation (RMSD) values remained largely stable over the time course of the MD simulation (RET^{wt} and RET^{V804M}), thus supporting our proposed model in which AD80 binds in the DFG-out conformation of the kinase (fig. S5A). In this model, AD80 forms a hydrogen bond (H-bond) with the aspartate of the DFG motif that may be involved in the stabilization of the DFG-out conformation (Fig. 3A). A similar H-bond is also observed for cabozantinib, a known type II inhibitor, bound to RET^{wt} (fig. S5B; see the Supplementary Materials and Methods for model generation). This finding corroborates the validity of our binding mode hypothesis, although the pose is biased by construction, being based on the refined RET^{wt}/AD80 structure. Furthermore, we developed a binding pose model for AD57 (derivative of AD80) bound to RET^{wt} (see below), which, upon superimposition, displays considerable similarity with the experimentally determined structure of AD57 bound to cSrc (PDB code 3EL8) in the DFG-out form, again validating our approach (figs. S4H and S5C). Next, we performed free energy MD simulations to transform AD80 into AD57. The calculations yielded a binding free energy difference of $\Delta\Delta G° = -0.21 \pm 0.17$ kcal mol^{-1} at 25°C, which compares well with the values derived from median inhibitory concentration (IC_{50}) in in vitro kinase measurements. These latter concentration-based measurements of binding affinity translate into an experimental estimate of the binding free energy difference of −0.41 kcal mol^{-1} with IC_{50}(AD57) of 2 nM and IC_{50}(AD80) of 4 nM (see the Supplementary Materials and Methods) (*13*). Using an integral equation approximation as an alternative computational approach, we obtained 0.1 kcal mol^{-1}, also in close correspondence with both the MD and experimental results. Thus, these analyses further support the proposed DFG-out conformation as the preferred binding mode because such agreement between the experiment and the theory would not have been expected if the true and predicted binding modes were largely dissimilar.

Overall, our cellular screening, phosphoproteomic, biochemical, and structural data indicate that potent type II inhibitors, such as AD80 or ponatinib, have an optimal RET-specific profile that distinguishes them from currently available anti-RET drugs.

Introduction of RET kinase gatekeeper mutation reveals differential activity of RET inhibitors

Secondary resistance mutations frequently target a conserved residue, termed gatekeeper, that controls access to a hydrophobic subpocket of

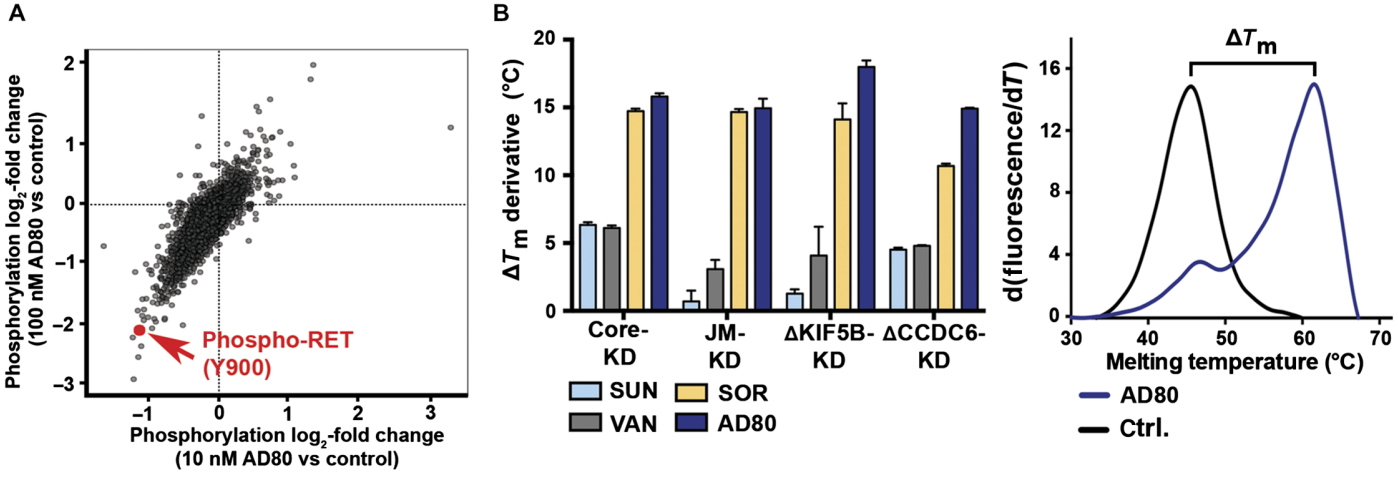

Fig. 2. AD80 specifically targets RET and tightly binds to RET fusion kinase. (**A**) Scatterplot of log_2-fold phosphorylation change for LC-2/AD cells treated (4 hours) with either 10 or 100 nM AD80. Each dot represents a single phosphosite; phospho-RET (Y900) is highlighted in red. (**B**) Difference in melting temperatures after AD80, sorafenib (SOR), vandetanib (VAN), or sunitinib (SUN) addition (ΔT_m) and the respective SEM are shown for each construct. Thermal shift experiments were performed using independent preparations of each protein and were carried out in triplicates (left). Representative thermal melting curves for ΔKIF5B-KD incubated with either AD80 (1 μM) or the equivalent volume of dimethyl sulfoxide (DMSO) (ctrl.) are shown (right).

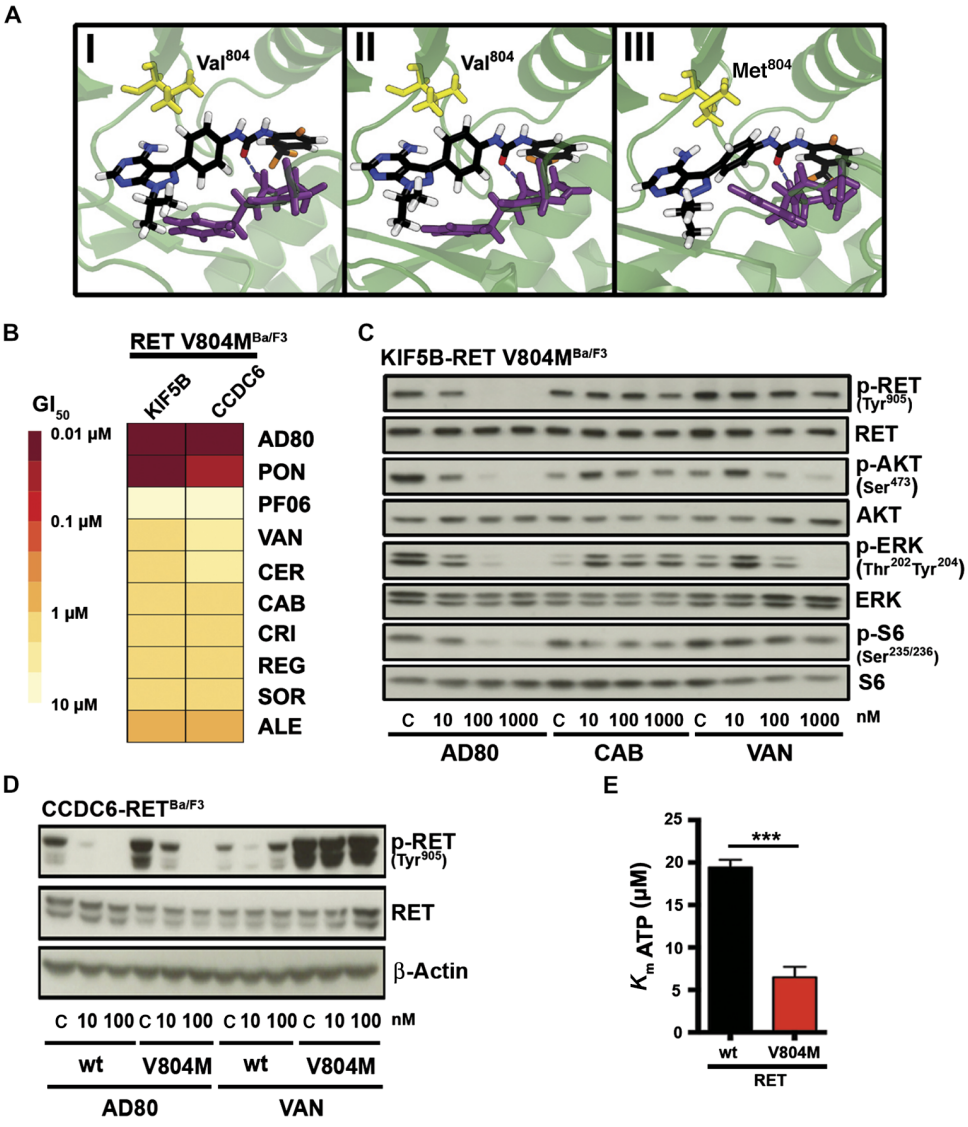

Fig. 3. AD80 is active against gatekeeper mutant RET^{V804M} cells. (**A**) Optimized structures after extensive MD refinement followed by ALPB optimization. (i) RET^{wt}/AD80 after 102 ns, (ii) RET^{wt}/AD57 after 202 ns (92 ns from RET^{wt}/AD80 simulation followed by 110 ns from TI-MD), and (iii) RET^{V804M}/AD80 after 107 ns (side view). The DFG motif is shown in violet. Distances from the center of central phenyl to Val^{804}-C(wt), Ile^{788}-C(wt), and Met^{804}-S(V804M) are 4.77, 3.90, and 4.29 Å, respectively. Dashed lines indicate the H-bond between the bound ligands and aspartate of the DFG motif. (**B**) Heat map of mean 50% growth inhibition (GI_{50}) values ($n \geq 3$) of Ba/F3 cells expressing CCDC6-RET^{V804M} or KIF5B-RET^{V804M} after 72 hours of treatment, as assessed for various inhibitors. (**C**) Immunoblotting of AD80-, cabozantinib-, or vandetanib-treated (4 hours) KIF5B-RET^{V804M} Ba/F3 cells. (**D**) Immunoblotting of Ba/F3 cells expressing CCDC6-RET-RET^{wt} or CCDC6-RET^{V804M} under AD80 or vandetanib treatment (4 hours). wt, wild type. (**E**) Calculated Michaelis constant (K_m) values of ATP binding to RET^{wt} or RET^{V804M} from three independent experiments. ***$P < 0.001$, $n = 3$.

the kinase domain (*21*). To test the impact of the gatekeeper resistance mutations on RET inhibitors, we established Ba/F3 cells expressing *KIF5B-RET^{V804M}* or *CCDC6-RET^{V804M}* and tested them against a panel of different drugs. As expected, only ponatinib and AD80 showed high activity in these gatekeeper mutant cells (Fig. 3B) (*22*). Similar activity was observed when testing the AD80 derivatives AD57 and AD81 for their inhibitory potential on Ba/F3 cells expressing wild-type and V804M-mutated *KIF5B-RET* or *CCDC6-RET* (fig. S6A). This effect was also evident in the ability of AD80 to inhibit phosphorylation of RET as well as of ERK, AKT, and S6K in these cells (Fig. 3C and table S1). Next, we used computational homology modeling coupled with MD refinement of AD80 in RET^{wt} in comparison with RET^{V804M}-mutant kinases. In line with our in vitro results, this analysis revealed high structural similarity and similar binding free energy estimates for both variants (-2.5 kcal mol^{-1} for transforming RET^{wt} to RET^{V804M} bound to AD80 from the integral equation model) (see Fig. 3A and the Supplementary Materials and Methods).

In parallel, we noticed that independent of the individual treatment, RET phosphorylation tended to be higher in gatekeeper mutant cells when compared to wild-type RET (Fig. 3D). To further characterize these differences, we performed in vitro kinase assays and found that the introduction of the *RET^{V804M}* mutation significantly ($P < 0.001$) increases the affinity of the recombinant receptor for adenosine 5′-triphosphate (ATP) when compared to the recombinant wild-type receptor (Fig. 3E). Thus, similar to gatekeeper-induced effects on ATP affinity observed for *EGFR^{T790M}* mutations, our data suggest that these effects may be of relevance for the activity of RET inhibitors in *KIF5B-RET^{V804M}* and *CCDC6-RET^{V804M}* cells (*23*).

Saturated mutagenesis screening identifies CCDC6-RET^{I788N} drug resistance mutation

To identify RET kinase mutations that may be associated with resistance against targeted therapy, we performed accelerated mutagenesis of *RET* fusion plasmids (*24*, *25*). We identified the *CCDC6-RET^{I788N}* mutation by selection of an AD80-resistant cell population (table S6). To validate this finding, we engineered Ba/F3 cells expressing *KIF5B-RET^{I788N}* or *CCDC6-RET^{I788N}* and observed a robust shift in cytotoxicity in response to AD80 treatment (Fig. 4A), as well as the other RET inhibitors, cabozantinib and vandetanib, but not ponatinib (Fig. 4B and fig. S6B). Immunoblotting confirmed that the introduction of the *KIF5B-RET^{I788N}* mutation had a minor effect on the efficacy of ponatinib but a major impact on AD80, as measured by phospho-RET analysis (Fig. 4, C and D). Computational binding mode analysis (Figs. 3A and 4E) suggests that both positions 804 and 788 are adjacent to the location of the central phenyl ring of AD80; characteristic distances between the phenyl center of mass and the nearest adjacent protein nonhydrogen sites to Val^{804}-C(wt), Ile^{788}-C(wt), Met^{804}-S(V804M), and Ile^{788}-C(V804M) are 4.77, 3.90, 4.29, and 4.61 Å, respectively. However, because V804M and I788N mutants responded differently to AD80, a clear conclusion about the molecular origin was

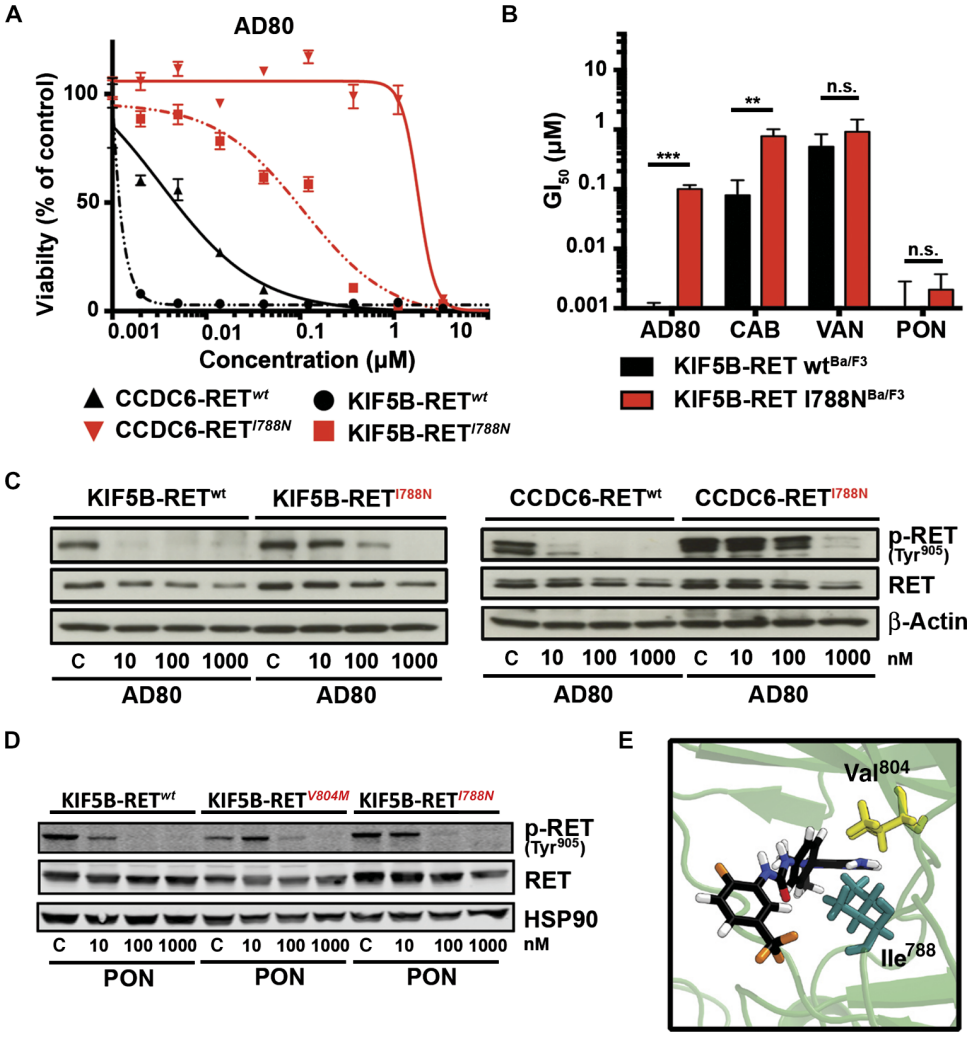

Fig. 4. RET^{I788N} mutations abrogate the activity of AD80 but not ponatinib. (**A**) Dose-response curves for AD80 against Ba/F3 cells expressing KIF5B-RET^{wt} (black) or KIF5B-RET^{I788N} (red) and CCDC6-RET^{wt} (black dashed line) or CCDC6-RET^{I788N} (red dashed line) ($n = 3$). (**B**) Bar graph of mean GI_{50} values + SD (from $n = 3$) for KIF5B-RET^{wt} or KIF5B-RET^{I788N} Ba/F3 cells treated (72 hours) with AD80, cabozantinib (CAB), vandetanib (VAN), or ponatinib (PON). ***$P < 0.001$; **$P < 0.01$; n.s., not significant. (**C**) Immunoblot of Ba/F3 cells expressing KIF5B-RET^{wt} or KIF5B-RET^{I788N} and CCDC6-RET^{wt} or CCDC6-RET^{I788N} treated (4 hours) with AD80. (**D**) Immunoblot of KIF5B-RET^{wt}, KIF5B-RET^{V804M}, or KIF5B-RET^{I788N} expressing Ba/F3 cells treated (4 hours) with ponatinib. HSP90 is used as loading control. (**E**) Optimized structure after extensive MD refinement followed by ALPB optimization. RET^{wt}/AD80 after 102 ns (side view). Distance from the center of central phenyl to Ile^{788}-C(V804M) is 4.61 Å.

not possible based on structural analysis alone, requiring further investigations. Thus, our data uncovered a resistance mutation RET^{I788N} that may arise in *RET*-rearranged tumors under RET inhibitor treatment and that retains sensitivity against ponatinib.

Feedback-induced activation of MAPK signaling modulates activity of RET inhibitors

Beyond the acquisition of secondary mutations, drug treatment of cancer cells may also release feedback loops that override the activity of targeted cancer treatment (*26*, *27*). To systematically characterize these effects, we analyzed altered gene expression by RNA-sequencing (RNA-seq) of LC-2/AD cells under AD80 treatment and performed gene set enrichment analysis (GSEA) (*28*). Our analyses revealed that treatment with AD80 results in up-regulation of genes that are typically repressed by active KRAS (KRAS down; adjusted $P < 0.0001$). On the contrary, genes that are activated by KRAS were down-regulated (KRAS up; adjusted $P = 0.003$) (Fig. 5A). Accordingly, the list of significantly down-regulated genes contained *DUSP6* (adjusted $P < 1 \times 10^{-250}$), *SPRY4* (adjusted $P = 5.75 \times 10^{-89}$), *DUSP5* (adjusted $P = 2.52 \times 10^{-38}$), and other genes that buffer mitogen-activated protein kinase (MAPK) pathway (Fig. 5B) (*29*). This transcriptional deregulation of MAPK signaling was accompanied by residual phospho-ERK staining in immunoblotting analyses of *RET*-rearranged LC-2/AD cells after 24 hours of inhibitor treatment (fig. S6C). Using a Group-based Prediction System (GPS 2.12) to identify kinase-specific phosphosites that are perturbed in AD80-treated LC-2/AD cells assessed in our mass spectrometry–based analysis, we identified a marked enrichment of phosphosites known from different families of noncanonical MAPK kinases (MEKs), such as MAPK8 (66 phosphosites), MAPK13 (21 phosphosites), or MAPK12 (15 phosphosites) (Fig. 5C).

We next tested the relevance of Ras-MAPK pathway reactivation in *RET*-rearranged cells treated with AD80 alone or a combination of AD80 and the MEK inhibitor trametinib. In TPC-1 cells with limited vulnerability to RET inhibition, we observed a pronounced phospho-ERK signal in cells after inhibition with AD80 when compared to LC-2/AD cells (fig. S6D). The combination of AD80 and trametinib fully abrogated MAPK signaling and depleted the outgrowth of resistant cells in clonogenic assays and enhanced the reduction of viability (Fig. 5D and fig. S6, E and F).

To formally test the relevance of MAPK pathway activation in the context of resistance to RET-targeted therapies in *RET*-rearranged cells, we stably transduced LC-2/AD cells with lentiviral *KRAS*^{G12V}. Introduction of the oncogenic *KRAS* allele into LC-2/AD cells largely eliminated the activity of AD80, as measured in viability assays and by staining of phospho-ERK (Fig. 5, E and F). Overall, our data suggest that drug-induced transcriptional and posttranslational reactivation of Ras-MAPK signaling may modulate the activity of RET-targeted inhibitors in *RET*-rearranged cells.

AD80 potently shrinks *RET*-rearranged tumors in patient-derived xenografts

To compare the in vivo efficacy of AD80 head-to-head with other RET inhibitors, we engrafted NIH-3T3 cells driven by CRISPR/Cas9-induced *KIF5B-RET* rearrangements into NSG (nonobese

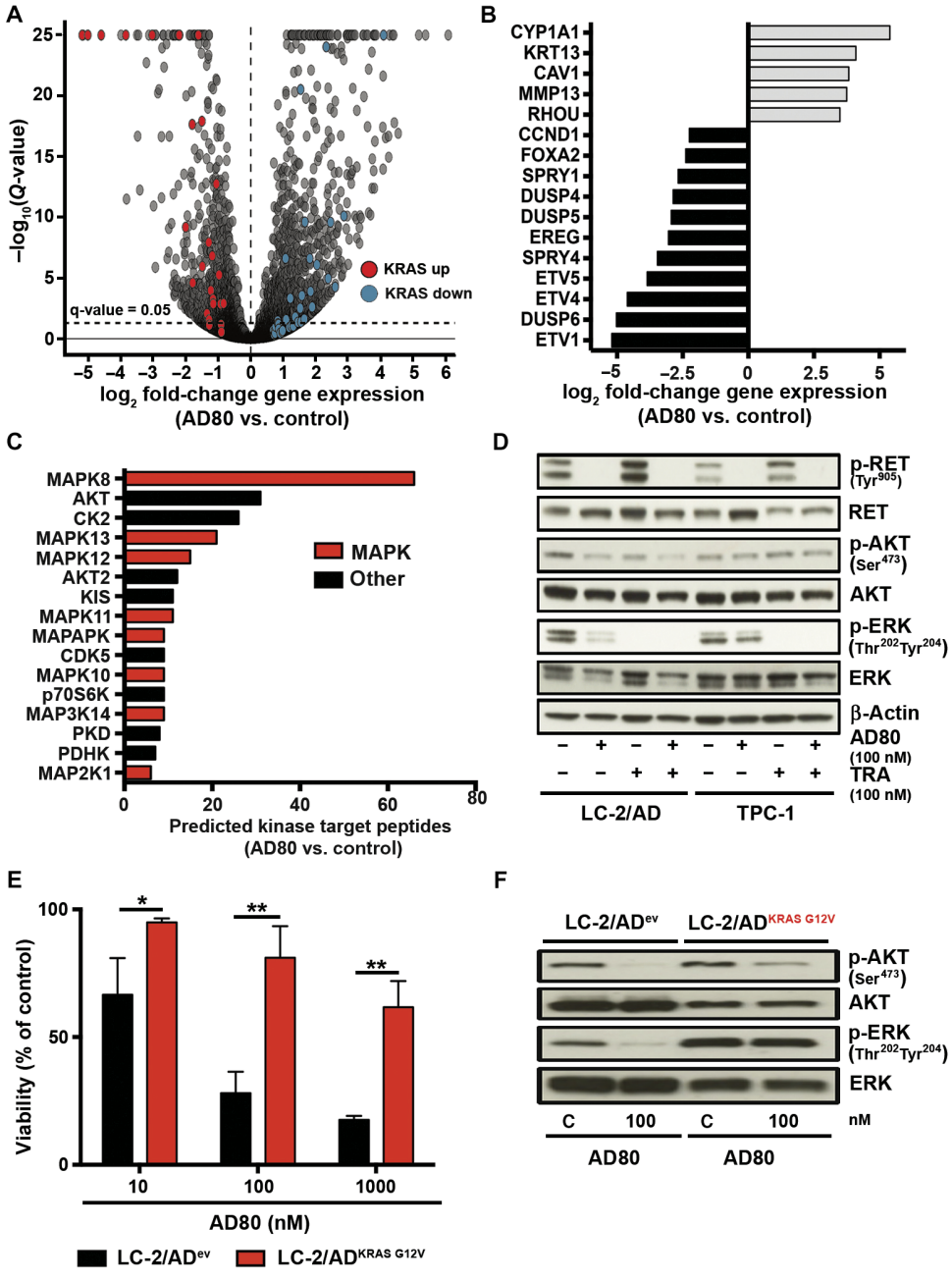

Fig. 5. MAPK pathway activation may be involved in the development of resistance against RET inhibition. (**A**) RNA-seq results of LC-2/AD cells treated (48 hours) with 100 nM AD80. Genes contained within the core enrichments of GSEA against the hallmark gene sets with genes up-regulated (KRAS up) or down-regulated (KRAS down) by active KRAS are highlighted by red and blue, respectively. The dashed line represents false discovery rate–adjusted *Q* value = 0.05. (**B**) Relevant genes from the top 50 genes with the strongest significant changes in RNA-seq after AD80 treatment (100 nM; 48 hours). (**C**) Predicted number of down-regulated phosphorylation sites for each kinase. All kinases with greater than or equal to six down-regulated phosphorylation sites are shown in hierarchical order. Kinases associated with MAPK pathway signaling are highlighted in red. (**D**) In immunoblotting assays, RET signaling was monitored in LC-2/AD and TPC-1 cells treated (48 hours) with AD80 (0.1 μM), trametinib (TRA) (0.1 μM), or a combination of both inhibitors. (**E**) LC-2/AD^{ev} or LC-2/AD$^{KRAS\ G12V}$ cells were treated (72 hours) with AD80. Results are shown as means + SD ($n = 3$). ***$P < 0.001$; **$P < 0.01$; *$P < 0.05$. (**F**) Immunoblotting of LC-2/AD^{ev} or LC-2/AD$^{KRAS\ G12V}$ cells under AD80 treatment (100 nM; 4 hours).

diabetic/severe combined immunodeficient gamma) mice. After the development of tumors, mice were treated with either vehicle or 12.5 to 25 mg/kg of AD80, cabozantinib, or vandetanib, and tumors were explanted 4 hours later (*30*, *31*). We observed a pronounced reduction in phosphorylation of RET as well as AKT and ERK in tumors treated with AD80 (25 mg/kg) but not in tumors treated with cabozantinib or vandetanib (Fig. 6A). Encouraged by these results, we next treated a cohort ($n = 16$) of patient-derived xenograft (PDX) mice engrafted with tumor tissue from a *CCDC6-RET*–rearranged colorectal cancer (CRC) patient with either vehicle or AD80 (25 mg/kg). Treatment with AD80 induced significant ($P < 0.001$) tumor shrinkage in CCDC6-RET PDX^{wt} (Fig. 6, B and C, and fig. S7A) (*32*). In line with our in vitro data for cells harboring *RET* gatekeeper mutations, tumor shrinkage ($P < 0.01$) was robust but less pronounced when we treated PDX mice ($n = 16$) engrafted with CRC tissue that had developed a *CCDC6-RET*^{V804M} gatekeeper mutation under ponatinib treatment (Fig. 6, B and D, and fig. S7B) (*33*). Furthermore, we observed a robust reduction of cellular proliferation (*CCDC6-RET*^{wt}, $P < 0.001$; *CCDC6-RET*^{V804M}, $P < 0.05$), as measured by KI-67 staining in *CCDC6-RET*^{wt} and *CCDC6-RET*^{V804M} tumors (Fig. 6, E and F). AD80 treatment did not cause body weight loss in either PDX model over the course of the study (fig. S7, C and D). Together, our data indicate that AD80 is a highly potent RET inhibitor with a favorable pharmacokinetic profile in clinically relevant *RET* fusion–driven tumor models.

DISCUSSION

Our chemical-genomic and chemical-proteomic analyses revealed three interesting findings with major implications for the development of effective therapies against *RET*-rearranged tumors: (i) *RET*-rearranged tumors show exquisite vulnerability to a subset of type II inhibitors that target the DFG-out conformation of RET kinase,

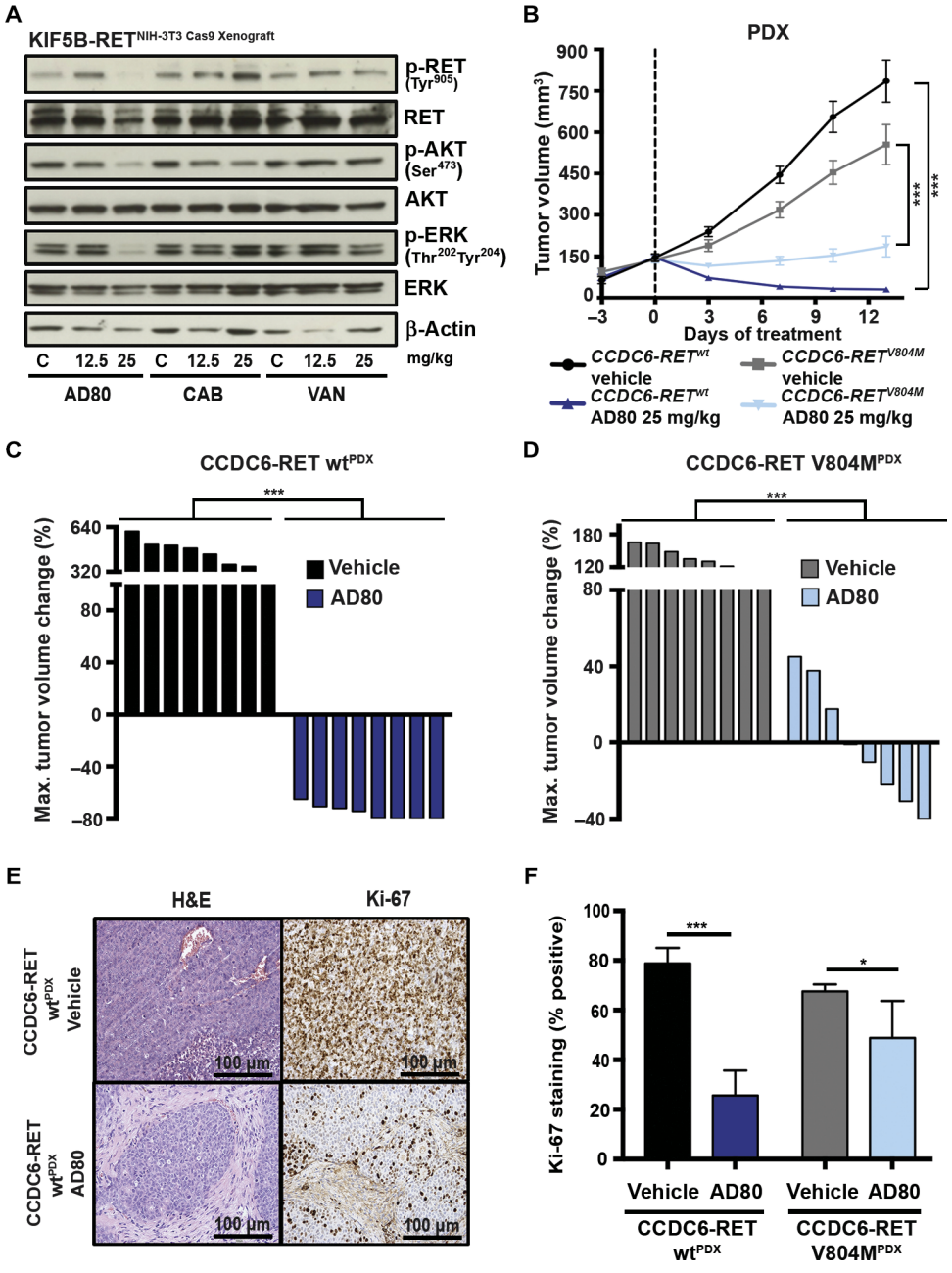

Fig. 6. AD80 treatment effectively shrinks *RET*-rearranged tumors in PDX models. (**A**) Immunoblotting of tumor tissue from CRISPR/Cas9-induced NIH-3T3$^{KIF5B\text{-}RET}$ xenografts was performed. Mice were treated (4 hours) with vehicle control or 12.5 or 25 mg/kg AD80, CAB, or VAN and were sacrificed. (**B**) Median tumor volume was assessed using consecutive measurements of PDX tumors driven by *CCDC6-RET*^{wt} or *CCDC6-RET*^{V804M} rearrangements under treatment with either AD80 (25 mg/kg; 14 days) or vehicle control (14 days). Treatment started at day 0. (**C**) Waterfall plot for each *CCDC6-RET*^{wt} fusion–positive PDX depicting best response (14 days) under AD80 or vehicle control treatment. ***$P < 0.001$. (**D**) Waterfall plot for each *CCDC6-RET*^{V804M}–positive PDX depicting best response (7 days) under AD80 or vehicle control treatment. ***$P < 0.001$. (**E**) Representative immunohistochemistry (IHC) staining for hematoxylin and eosin (H&E) and Ki-67 of AD80- or vehicle control–treated *CCDC6-RET*^{wt} PDX. Scale bars, 100 µm. (**F**) Quantification of Ki-67 IHC staining. ***$P < 0.001$; *$P < 0.05$.

The repurposing of crizotinib for the targeted treatment of *ALK*-rearranged tumors enabled a fast-track introduction of precision cancer medicine for this group of cancer patients and raised hopes that this approach may be a blueprint for the targeted treatment of other driver oncogenes, such as RET (*34*). Although initial clinical response rates were promising in selected patients, a median progression-free survival of less than 6 months and response rates of only about 18% in retrospective studies indicated that *RET* may be a difficult drug target after all (*7*, *9*, *10*, *35*).

Our systematic characterization of anti-RET drugs revealed distinct activity and specificity profiles for the type II kinase inhibitors AD80 and ponatinib in independent in vitro and in vivo models across different lineages of *RET*-rearranged cancer. This finding is noteworthy because the biochemical profiling of these compounds and structurally related compounds would have suggested a broad spectrum of kinase targets (*13*, *36*, *37*). Our data also suggest that an inhibitory profile, including a stable binding in the DFG-out conformation of RET together with a potent in vitro kinase activity, may predict efficacy against *RET*-rearranged cancer cells. At the same time, our study is limited through the lack of insight into drug residence time or structural kinetics that may also contribute to the overall activity of type II inhibitors such as sorafenib and other RET inhibitors (*20*, *38*).

Notably, we identified a *CCDC6-RET*^{I788N} resistance mutation that renders a number of tested RET inhibitors ineffective while retaining vulnerability to ponatinib. These findings resemble the experience with ALK inhibitors in *ALK*-rearranged tumors, where the availability of potent inhibitors allows a mutant-specific selection of inhibitors to overcome drug resistance (*39*). In addition, our results suggest that the reactivation of intracellular networks, including MAPK signaling, may contribute to drug tolerance and, over time, may modulate the efficacy of RET kinase inhibitors in *RET*-rearranged tumors. Given the evident clinical need for effective targeted drugs against RET, our results provide a strong rationale for optimization of current therapeutic strategies and development of RET inhibitors for the effective treatment of *RET*-rearranged cancers.

(ii) compound specificity and compound activity can be faithfully determined in complementary in vitro and in vivo models of rearranged RET, and (iii) resistance mechanisms against targeted inhibition of RET may involve *RET*^{I788N} mutations and the reactivation of MAPK signaling.

MATERIALS AND METHODS

Study design

The goal of our study was to systematically profile a series of kinase inhibitors to identify features that predict high activity against *RET*-rearranged tumors. In particular, we characterized the role of inhibitor binding to RET kinase. Furthermore, we performed chemical genomic analyses and transcriptional profiling to identify mechanisms of resistance against RET inhibitors in *RET*-rearranged cancer cells.

The selection of cell lines was based on availability of *RET*-rearranged cellular models. We used the *RET*-rearranged lung adenocarcinoma cell line LC2/AD and the *KIF5B-RET* and *CCDC6-RET* viral transduced Ba/F3 pro B cell line to benchmark the differential activity of different RET inhibitors. We specifically focused on the characterization of AD80 and ponatinib as the most active drugs. To further profile the intracellular effects of AD80, we used phosphoproteomics to demonstrate that phospho-RET is among the most decreased detected peptides. Because it was not possible for us to obtain crystal structures of AD80 in a complex with RET, we used homology-based modeling of the AD80:RET complex to further substantiate our hypothesis of AD080 binding the DFG-out conformation of RET. To identify resistance mutations against AD80 in *CCDC6-RET*, we performed saturated mutagenesis screening and found a I788N mutation but no mutations at the gatekeeper position V804 of RET. Finally, we used murine PDX models driven by *CCDC6-RET*^{wt} or *CCDC6-RET*^{V804M} showing potent in vivo efficacy of AD80. All experiments were performed at least three times. Screenings were performed in triplicates within each experiment. IHC analyses of PDX tumors were randomly selected and reviewed in a blinded fashion. More details for each individual experiment are indicated in Materials and Methods as well as in the main text and figure legends.

CRISPR/Cas9

CRISPR technology was used via a pLenti vector containing Cas9-IRES-blasticidine and two U6 promoters for expression of individual single-guide RNAs (sgRNAs) [sgRNA1 (intron 15 murine *KIF5B*), GGCACCAAACACTTCACCCC; sgRNA2 (intron 11 murine *RET*), GGGTGTAGCGAAGTGTGCAT) (*14*)]. Twenty-four hours after transfection, the medium was changed to medium supplemented with blasticidin (10 μg/ml) (Life Technologies) for 4 days.

Immunoblot analyses

Immunoblot analyses were performed as previously described (*40*). The individual antibodies are specified in the Supplementary Materials and Methods. Detection of proteins was performed via horseradish peroxidase or via near-infrared fluorescent antibodies using a LI-COR Odyssey CLx imaging system.

Phosphoproteomic analyses

LC-2/AD cells were treated with 0, 10, or 100 nM AD80, lysed, proteolytically digested with trypsin, and labeled with an isobaric mass tag (TMT10plex, Thermo Fisher Scientific). Peptides for global proteome analysis were fractionated by high-pH reversed-phase chromatography. Phosphopeptides were enriched via TiO_2 beads and fractionated using hydrophilic interaction chromatography (*41*). Fractions were analyzed by nano-liquid chromatography–tandem mass spectrometry on a Q Exactive HF mass spectrometer (Thermo Fisher Scientific), and data were analyzed using the Proteome Discoverer 1.4 software (Thermo Fisher Scientific). A detailed description can be found in the Supplementary Materials and Methods.

Protein thermal shift assay

Different variants of RET kinase domain were designed and ordered from GeneArt (Life Technologies). RET variants were expressed in SF21 cells and harvested 72 hours after transfection. Subsequently, proteins were purified and phosphorylated. To determine the protein thermal shift, protein variants were incubated with DMSO or 1 μM compound. SYPRO Orange dye (Life Technologies) was added to each drug-treated sample, and thermal shift was measured in a 7500 Fast Real-Time PCR machine (Applied Biosystems) in a temperature range of 25° to 90°C. Subsequent analysis was performed using Protein Thermal Shift Software v1.2 (Applied Biosystems). A detailed description can be found in the Supplementary Materials and Methods.

Computational binding mode modeling

Briefly, VEGFR was taken as a template for modeling and filling of sequence gaps, representing the relevant part of the wild-type RET protein. All ligand-bound models were created by superpositioning, followed by extensive MD simulations and energy minimization to relax the structures (RET^{wt}/AD80, RET^{V804M}/AD80, and RET^{wt}/cabozantinib). For comparison with experimentally determined IC_{50} ratios, the binding free energy difference between RET^{wt}/AD80 and RET^{wt}/AD57 was further estimated by MD simulations and integral equation calculations (*42*). The latter approach was also used for approximate determination of the impact of the V804M mutation on the binding affinity of AD80. A detailed description can be found in the Supplementary Materials and Methods.

ATP-binding constant determination

ATP K_m determination for RET^{wt} and RET^{V804M} mutant was performed using the HTRF KinEASE TK assay (Cisbio) according to the manufacturer's instructions. To determine ATP K_m, wild type and V804M mutant were incubated with different ATP concentrations (300 μM to 1.7 nM) for 20 min (RET^{wt}) or 15 min (RET^{V804M}). Phosphorylation of the substrate peptide was determined by Förster resonance energy transfer between europium cryptate and XL665. ATP K_m (app) was calculated using a Michaelis-Menten plot.

Patient-derived xenografts

Tumor fragments from stock mice (BALB/c nude) inoculated with *CCDC6-RET* fusion–positive patient-derived tumor tissues (provided by Crown Bioscience Inc.) were harvested and used for propagation into BALB/c nude mice (*32*). Mice were randomly allocated into vehicle (5% DMSO and 40% PEG400 in saline)– and AD80 (25 mg/kg)–treated groups (oral gavage) when the average tumor volume reached 100 to 200 mm^3. Tumor volume was measured twice weekly in two dimensions using a caliper, and the volume is expressed in cubic millimeters [$TV = 0.5(a \times b^2)$, where a and b represent long and short diameter, respectively].

Immunohistochemistry

IHC was performed on Leica BOND automated staining systems using Ki-67 and Mib-1 (Dako) antibodies according to the manufacturer's instructions. Ki-67 labeling index was determined by manually counting 100 tumor cells in the area of the highest proliferation.

Statistical analysis

All statistical analyses were performed using Microsoft Excel 2011 or GraphPad Prism 6.0h for Mac or R (www.r-project.org/). P values were assessed using Student's t test, unless specified otherwise. Significance is marked with $^*P \leq 0.05$, $^{**}P \leq 0.01$, or $^{***}P \leq 0.001$.

SUPPLEMENTARY MATERIALS

www.sciencetranslationalmedicine.org/cgi/content/full/9/394/eaah6144/DC1

Materials and Methods

Fig. S1. Selective inhibition of signaling induced by rearranged RET and clinical activity in vivo.

Fig. S2. Induction of *KIF5B-RET* rearrangements in NIH-3T3 cells via CRISPR/Cas9 and S6 kinase as an off-target of AD80.

Fig. S3. Characterization of the activity profile of AD80.

Fig. S4. Delineation of the cellular targets of AD80 using ligand screens and thermal shift experiments.

Fig. S5. RMSD of RET and AD80 or cabozantinib over time and ALPB-optimized structures.

Fig. S6. Inhibitory potential of AD80 derivatives and resistance mechanisms against RET inhibition.

Fig. S7. Validation of PDX via fluorescent in situ hybridization (FISH) and in vivo effects induced by treatment with AD80.

Table S1. IC_{50} values of AD80, cabozantinib, and vandetanib for phospho-RET in Ba/F3 cells expressing wild type or V804M *KIF5B-RET*.

Table S2. Rates of clinical response to currently available anti-RET drugs and clinical information of patients used in retrospective analysis.

Table S3. GI_{50} values of the panel of patient-derived cell lines.

Table S4. Tabulated derivative melting temperatures (T_m) and differences in melting temperature (ΔT_m) values.

Table S5. In vitro kinase assay of RET^{wt}, RET^{V804M}, and RET^{V804L} mutants with different inhibitors.

Table S6. Experimental setup for saturated mutagenesis screening.

References (*43*–*66*)

REFERENCES AND NOTES

1. D. Lipson, M. Capelletti, R. Yelensky, G. Otto, A. Parker, M. Jarosz, J. A. Curran, S. Balasubramanian, T. Bloom, K. W. Brennan, A. Donahue, S. R. Downing, G. M. Frampton, L. Garcia, F. Juhn, K. C. Mitchell, E. White, J. White, Z. Zwirko, T. Peretz, H. Nechushtan, L. Soussan-Gutman, J. Kim, H. Sasaki, H. R. Kim, S.-i. Park, D. Ercan, C. E. Sheehan, J. S. Ross, M. T. Cronin, P. A. Jänne, P. J. Stephens, Identification of new *ALK* and *RET* gene fusions from colorectal and lung cancer biopsies. *Nat. Med.* **18**, 382–384 (2012).
2. K. Takeuchi, M. Soda, Y. Togashi, R. Suzuki, S. Sakata, S. Hatano, R. Asaka, W. Hamanaka, H. Ninomiya, H. Uehara, Y. Lim Choi, Y. Satoh, S. Okumura, K. Nakagawa, H. Mano, Y. Ishikawa, RET, ROS1 and ALK fusions in lung cancer. *Nat. Med.* **18**, 378–381 (2012).
3. T. Kohno, H. Ichikawa, Y. Totoki, K. Yasuda, M. Hiramoto, T. Nammo, H. Sakamoto, K. Tsuta, K. Furuta, Y. Shimada, R. Iwakawa, H. Ogiwara, T. Oike, M. Enari, A. J. Schetter, H. Okayama, A. Haugen, V. Skaug, S. Chiku, I. Yamanaka, Y. Arai, S.-i. Watanabe, I. Sekine, S. Ogawa, C. C. Harris, H. Tsuda, T. Yoshida, J. Yokota, T. Shibata, *KIF5B-RET* fusions in lung adenocarcinoma. *Nat. Med.* **18**, 375–377 (2012).
4. T. Kodama, T. Tsukaguchi, Y. Satoh, M. Yoshida, Y. Watanabe, O. Kondoh, H. Sakamoto, Alectinib shows potent antitumor activity against *RET*-rearranged non–small cell lung cancer. *Mol. Cancer Ther.* **13**, 2910–2918 (2014).
5. R. Kurzrock, S. I. Sherman, D. W. Ball, A. A. Forastiere, R. B. Cohen, R. Mehra, D. G. Pfister, E. E. W. Cohen, L. Janisch, F. Nauling, D. S. Hong, C. S. Ng, L. Ye, R. F. Gagel, J. Frye, T. Müller, M. J. Ratain, R. Salgia, Activity of XL184 (Cabozantinib), an oral tyrosine kinase inhibitor, in patients with medullary thyroid cancer. *J. Clin. Oncol.* **29**, 2660–2666 (2011).
6. M. G. Borrello, E. Ardini, L. D. Locati, A. Greco, L. Licitra, M. A. Pierotti, RET inhibition: Implications in cancer therapy. *Expert Opin. Ther. Targets* **17**, 403–419 (2013).
7. A. Drilon, L. Wang, A. Hasanovic, Y. Suehara, D. Lipson, P. Stephens, J. Ross, V. Miller, M. Ginsberg, M. F. Zakowski, M. G. Kris, M. Ladanyi, N. Rizvi, Response to Cabozantinib in patients with *RET* fusion-positive lung adenocarcinomas. *Cancer Discov.* **3**, 630–635 (2013).
8. G. S. Falchook, N. G. Ordóñez, C. C. Bastida, P. J. Stephens, V. A. Miller, L. Gaido, T. Jackson, D. D. Karp, Effect of the RET inhibitor vandetanib in a patient with RET fusion–positive metastatic non–small-cell lung cancer. *J. Clin. Oncol.* **34**, e141–e144 (2016).
9. O. Gautschi, J. Milia, T. Filleron, J. Wolf, D. P. Carbone, D. Owen, R. Camidge, V. Narayanan, R. C. Doebele, B. Besse, J. Remon-Masip, P. A. Jänne, M. M. Awad, N. Peled, C.-C. Byoung, D. D. Karp, M. Van Den Heuvel, H. A. Wakelee, J. W. Neal, T. S. K. Mok, J. C. H. Yang, S.-H. I. Ou, G. Pall, P. Froesch, G. Zalcman, D. R. Gandara, J. W. Riess, V. Velcheti, K. Zeidler, J. Diebold, M. Früh, S. Michels, I. Monnet, S. Popat, R. Rosell, N. Karachaliou, S. I. Rothschild, J.-Y. Shih, A. Warth, T. Muley, F. Cabillic, J. Maziéres, A. Drilon, Targeting RET in patients with *RET*-rearranged lung cancers: Results from the global, multicenter *RET* registry. *J. Clin. Oncol.* **35**, 1403–1410 (2017).
10. K. Yoh, T. Seto, M. Satouchi, M. Nishio, N. Yamamoto, H. Murakami, N. Nogami, S. Matsumoto, T. Kohno, K. Tsuta, K. Tsuchihara, G. Ishii, S. Nomura, A. Sato, A. Ohtsu, Y. Ohe, K. Goto, Vandetanib in patients with previously treated *RET*-rearranged advanced non-small-cell lung cancer (LURET): An open-label, multicentre phase 2 trial. *Lancet Respir. Med.* **5**, 42–50 (2017).
11. T. Cascone, K. R. Hess, S. Piha-Paul, D. S. Hong, I. M. Subblah, T. Bhatt, A. Lui, S. Fu, A. Naing, F. Janku, D. D. Karp, F. Meric-Bernstam, J. V. Heymach, V. Subblah, Safety, toxicity and activity of multi-kinase inhibitor vandetanib in combination with everolimus in advanced solid tumors, paper presented at the 2016 ASCO Annual Meeting (2016).
12. M. Song, Progress in discovery of KIF5B-RET kinase inhibitors for the treatment of non-small-cell lung cancer. *J. Med. Chem.* **58**, 3672–3681 (2015).
13. A. C. Dar, T. K. Das, K. M. Shokat, R. L. Cagan, Chemical genetic discovery of targets and anti-targets for cancer polypharmacology. *Nature* **486**, 80–84 (2012).
14. P. S. Choi, M. Meyerson, Targeted genomic rearrangements using CRISPR/Cas technology. *Nat. Commun.* **5**, 3728 (2014).
15. M. Suzuki, H. Makinoshima, S. Matsumoto, A. Suzuki, S. Mimaki, K. Matsushima, K. Yoh, K. Goto, Y. Suzuki, G. Ishii, A. Ochiai, K. Tsuta, T. Shibata, T. Kohno, H. Esumi, K. Tsuchihara, Identification of a lung adenocarcinoma cell line with CCDC6-RET fusion gene and the effect of RET inhibitors in vitro and in vivo. *Cancer Sci.* **104**, 896–903 (2013).
16. M. L. Sos, K. Michel, T. Zander, J. Weiss, P. Frommolt, M. Peifer, D. Li, R. Ullrich, M. Koker, F. Fischer, T. Shimamura, D. Rauh, C. Mermel, S. Fischer, I. Stückrath, S. Heynck, R. Beroukhim, W. Lin, W. Winckler, K. Shah, T. LaFramboise, W. F. Moriarty, M. Hanna, L. Tolosi, J. Rahnenführer, R. Verhaak, D. Chiang, G. Getz, M. Hellmich, J. Wolf, L. Girard, M. Peyton, B. A. Weir, T.-H. Chen, H. Greulich, J. Barretina, G. I. Shapiro, L. A. Garraway, A. F. Gazdar, J. D. Minna, M. Meyerson, K.-K. Wong, R. K. Thomas, Predicting drug susceptibility of non–small cell lung cancers based on genetic lesions. *J. Clin. Invest.* **119**, 1727–1740 (2009).
17. P. P. Knowles, J. Murray-Rust, S. Kjær, R. P. Scott, S. Hanrahan, M. Santoro, C. F. Ibáñez, N. Q. McDonald, Structure and chemical inhibition of the RET tyrosine kinase domain. *J. Biol. Chem.* **281**, 33577–33587 (2006).
18. S. Müller, A. Chaikuad, N. S. Gray, S. Knapp, The ins and outs of selective kinase inhibitor development. *Nat. Chem. Biol.* **11**, 818–821 (2015).
19. M. Hasegawa, N. Nishigaki, Y. Washio, K. Kano, P. A. Harris, H. Sato, I. Mori, R. I. West, M. Shibahara, H. Toyoda, L. Wang, R. T. Nolte, J. M. Veal, M. Cheung, Discovery of novel benzimidazoles as potent inhibitors of TIE-2 and VEGFR-2 tyrosine kinase receptors. *J. Med. Chem.* **50**, 4453–4470 (2007).
20. B. Frett, F. Carlomagno, M. L. Moccia, A. Brescia, G. Federico, V. De Falco, B. Admire, Z. Chen, W. Qi, M. Santoro, H.-y. Li, Fragment-based discovery of a dual pan-RET/VEGFR2 kinase inhibitor optimized for single-agent polypharmacology. *Angew. Chem. Int. Ed.* **54**, 8717–8721 (2015).
21. F. Carlomagno, T. Guida, S. Anaganti, G. Vecchio, A. Fusco, A. J. Ryan, M. Billaud, M. Santoro, Disease associated mutations at valine 804 in the RET receptor tyrosine kinase confer resistance to selective kinase inhibitors. *Oncogene* **23**, 6056–6063 (2004).
22. L. Mologni, S. Redaelli, A. Morandi, I. Plaza-Menacho, C. Gambacorti-Passerini, Ponatinib is a potent inhibitor of wild-type and drug-resistant gatekeeper mutant RET kinase. *Mol. Cell. Endocrinol.* **377**, 1–6 (2013).
23. C.-H. Yun, K. E. Mengwasser, A. V. Toms, M. S. Woo, H. Greulich, K.-K. Wong, M. Meyerson, M. J. Eck, The T790M mutation in EGFR kinase causes drug resistance by increasing the affinity for ATP. *Proc. Natl. Acad. Sci. U.S.A.* **105**, 2070–2075 (2008).
24. M. Azam, R. R. Latek, G. Q. Daley, Mechanisms of autoinhibition and STI-571/imatinib resistance revealed by mutagenesis of *BCR-ABL*. *Cell* **112**, 831–843 (2003).
25. J. M. Heuckmann, M. Hölzel, M. L. Sos, S. Heynck, H. Balke-Want, M. Koker, M. Peifer, J. Weiss, C. M. Lovly, C. Grütter, D. Rauh, W. Pao, R. K. Thomas, ALK mutations conferring differential resistance to structurally diverse ALK inhibitors. *Clin. Cancer Res.* **17**, 7394–7401 (2011).
26. M. L. Sos, R. S. Levin, J. D. Gordan, J. A. Oses-Prieto, J. T. Webber, M. Salt, B. Hann, A. L. Burlingame, F. McCormick, S. Bandyopadhyay, K. M. Shokat, Oncogene mimicry as a mechanism of primary resistance to BRAF inhibitors. *Cell Rep.* **8**, 1037–1048 (2014).
27. S. Chandarlapaty, Negative feedback and adaptive resistance to the targeted therapy of cancer. *Cancer Discov.* **2**, 311–319 (2012).
28. A. Subramanian, P. Tamayo, V. K. Mootha, S. Mukherjee, B. L. Ebert, M. A. Gillette, A. Paulovich, S. L. Pomeroy, T. R. Golub, E. S. Lander, J. P. Mesirov, Gene set enrichment analysis: A knowledge-based approach for interpreting genome-wide expression profiles. *Proc. Natl. Acad. Sci. U.S.A.* **102**, 15545–15550 (2005).
29. C. A. Pratilas, B. S. Taylor, Q. Ye, A. Viale, C. Sander, D. B. Solit, N. Rosen, ^{V600}EBRAF is associated with disabled feedback inhibition of RAF–MEK signaling and elevated transcriptional output of the pathway. *Proc. Natl. Acad. Sci. U.S.A.* **106**, 4519–4524 (2009).
30. R. de Boer, Y. Humblet, J. Wolf, L. Nogová, K. Ruffert, T. Milenkova, R. Smith, A. Godwood, J. Vansteenkiste, An open-label study of vandetanib with pemetrexed in patients with previously treated non-small-cell lung cancer. *Ann. Oncol.* **20**, 486–491 (2009).
31. F. Bentzien, M. Zuzow, N. Heald, A. Gibson, Y. Shi, L. Goon, P. Yu, S. Engst, W. Zhang, D. Huang, L. Zhao, V. Vysotskaia, F. Chu, R. Bautista, B. Cancilla, P. Lamb, A. H. Joly, F. M. Yakes, In vitro and in vivo activity of cabozantinib (XL184), an inhibitor of RET, MET, and VEGFR2, in a model of medullary thyroid cancer. *Thyroid* **23**, 1569–1577 (2013).
32. J. M. Gozgit, T.-H. Chen, T. Clackson, V. M. Rivera, RET fusions identified in colorectal cancer PDX models are sensitive to the potent RET inhibitor ponatinib. *Cancer Res.* **74**, 2726 (2014).

33. M. Yang, J. Cai, S. Guo, J.-P. Wery, H. Q. Li, Rapid conversion to resistance, of a colon PDX with ret-fusion, by ponatinib treatment could potentially be attributed to the introduction of the gate keeper mutation V804M. *Cancer Res.* **75**, 3581 (2015).
34. B. J. Solomon, T. Mok, D.-W. Kim, Y.-L. Wu, K. Nakagawa, T. Mekhail, E. Felip, F. Cappuzzo, J. Paolini, T. Usari, S. Iyer, A. Reisman, K. D. Wilner, J. Tursi, F. Blackhall, First-line crizotinib versus chemotherapy in *ALK*-positive lung cancer. *N. Engl. J. Med.* **371**, 2167–2177 (2014).
35. O. Gautschi, T. Zander, F. A. Keller, K. Strobel, A. Hirschmann, S. Aebi, J. Diebold, A patient with lung adenocarcinoma and RET fusion treated with vandetanib. *J. Thorac. Oncol.* **8**, e43–e44 (2013).
36. A. C. Dar, M. S. Lopez, K. M. Shokat, Small molecule recognition of c-Src via the imatinib-binding conformation. *Chem. Biol.* **15**, 1015–1022 (2008).
37. T. O'Hare, W. C. Shakespeare, X. Zhu, C. A. Eide, V. M. Rivera, F. Wang, L. T. Adrian, T. Zhou, W.-S. Huang, Q. Xu, C. A. Metcalf III, J. W. Tyner, M. M. Loriaux, A. S. Corbin, S. Wardwell, Y. Ning, J. A. Keats, Y. Wang, R. Sundaramoorthi, M. Thomas, D. Zhou, J. Snodgrass, L. Commodore, T. K. Sawyer, D. C. Dalgarno, M. W. N. Deininger, B. J. Druker, T. Clackson, AP24534, a pan-BCR-ABL inhibitor for chronic myeloid leukemia, potently inhibits the T315I mutant and overcomes mutation-based resistance. *Cancer Cell* **16**, 401–412 (2009).
38. F. Carlomagno, S. Anaganti, T. Guida, G. Salvatore, G. Troncone, S. M. Wilhelm, M. Santoro, BAY 43-9006 inhibition of oncogenic RET mutants. *J. Natl. Cancer Inst.* **98**, 326–334 (2006).
39. J. F. Gainor, L. Dardaei, S. Yoda, L. Friboulet, I. Leshchiner, R. Katayama, I. Dagogo-Jack, S. Gadgeel, K. Schultz, M. Singh, E. Chin, M. Parks, D. Lee, R. H. DiCecca, E. Lockerman, T. Huynh, J. Logan, L. L. Ritterhouse, L. P. Le, A. Muniappan, S. Digumarthy, C. Channick, C. Keyes, G. Getz, D. Dias-Santagata, R. S. Heist, J. Lennerz, L. V. Sequist, C. H. Benes, A. J. Iafrate, M. Mino-Kenudson, J. A. Engelman, A. T. Shaw, Molecular mechanisms of resistance to first- and second-generation ALK inhibitors in *ALK*-rearranged lung cancer. *Cancer Discov.* **6**, 1118–1133 (2016).
40. L. Fernandez-Cuesta, D. Plenker, H. Osada, R. Sun, R. Menon, F. Leenders, S. Ortiz-Cuaran, M. Peifer, M. Bos, J. Daßler, F. Malchers, J. Schöttle, W. Vogel, I. Dahmen, M. Koker, R. T. Ullrich, G. M. Wright, P. A. Russell, Z. Wainer, B. Solomon, E. Brambilla, H. Nagy-Mignotte, D. Moro-Sibilot, C. G. Brambilla, S. Lantuejoul, J. Altmüller, C. Becker, P. Nürnberg, J. M. Heuckmann, E. Stoelben, I. Petersen, J. H. Clement, J. Sänger, L. A. Muscarella, A. la Torre, V. M. Fazio, I. Lahortiga, T. Perera, S. Ogata, M. Parade, D. Brehmer, M. Vingron, L. C. Heukamp, R. Buettner, T. Zander, J. Wolf, S. Perner, S. Ansén, S. A. Haas, Y. Yatabe, R. K. Thomas, *CD74–NRG1* fusions in lung adenocarcinoma. *Cancer Discov.* **4**, 415–422 (2014).
41. C. Dickhut, S. Radau, R. P. Zahedi, Fast, efficient, and quality-controlled phosphopeptide enrichment from minute sample amounts using titanium dioxide. *Methods Mol. Biol.* **1156**, 417–430 (2014).
42. J. Heil, S. M. Kast, 3D RISM theory with fast reciprocal-space electrostatics. *J. Chem. Phys.* **142**, 114107 (2015).
43. J. R. Wiśniewski, A. Zougman, N. Nagaraj, M. Mann, Universal sample preparation method for proteome analysis. *Nat. Methods* **6**, 359–362 (2009).
44. L. Kollipara, R. P. Zahedi, Protein carbamylation: In vivo modification or in vitro artefact? *Proteomics* **13**, 941–944 (2013).
45. J. M. Burkhart, C. Schumbrutzki, S. Wortelkamp, A. Sickmann, R. P. Zahedi, Systematic and quantitative comparison of digest efficiency and specificity reveals the impact of trypsin quality on MS-based proteomics. *J. Proteomics* **75**, 1454–1462 (2012).
46. K. Engholm-Keller, P. Birck, J. Størling, F. Pociot, T. Mandrup-Poulsen, M. R. Larsen, TiSH—A robust and sensitive global phosphoproteomics strategy employing a combination of TiO_2, SIMAC, and HILIC. *J. Proteomics* **75**, 5749–5761 (2012).
47. T. Taus, T. Köcher, P. Pichler, C. Paschke, A. Schmidt, C. Henrich, K. Mechtler, Universal and confident phosphorylation site localization using phosphoRS. *J. Proteome Res.* **10**, 5354–5362 (2011).
48. M. Spivak, J. Weston, L. Bottou, L. Käll, W. S. Noble, Improvements to the percolator algorithm for peptide identification from shotgun proteomics data sets. *J. Proteome Res.* **8**, 3737–3745 (2009).
49. Y. Xue, J. Ren, X. Gao, C. Jin, L. Wen, X. Yao, GPS 2.0, a tool to predict kinase-specific phosphorylation sites in hierarchy. *Mol. Cell. Proteomics* **7**, 1598–1608 (2008).
50. MODELLER; https://salilab.org/modeller/.
51. G. Sigalov, A. Fenley, A. Onufriev, Analytical electrostatics for biomolecules: Beyond the generalized Born approximation. *J. Chem. Phys.* **124**, 124902 (2006).
52. Amber; http://ambermd.org/.
53. J. Engel, A. Richters, M. Getlik, S. Tomassi, M. Keul, M. Termathe, J. Lategahn, C. Becker, S. Mayer-Wrangowski, C. Grütter, N. Uhlenbrock, J. Krüll, N. Schaumann, S. Eppmann, P. Kibies, F. Hoffgaard, J. Heil, S. Menninger, S. Ortiz-Cuaran, J. M. Heuckmann, V. Tinnefeld, R. P. Zahedi, M. L. Sos, C. Schultz-Fademrecht, R. K. Thomas, S. M. Kast, D. Rauh, Targeting drug resistance in EGFR with covalent inhibitors: A structure-based design approach. *J. Med. Chem.* **58**, 6844–6863 (2015).
54. W. L. Jorgensen, J. Chandrasekhar, J. D. Madura, R. W. Impey, M. L. Klein, Comparison of simple potential functions for simulating liquid water. *J. Chem. Phys.* **79**, 926–935 (1983).
55. NAMD; www.ks.uiuc.edu/Research/namd/.
56. D. Beglov, B. Roux, An integral equation to describe the solvation of polar molecules in liquid water. *J. Phys. Chem. B* **101**, 7821–7826 (1997).
57. A. Kovalenko, F. Hirata, Three-dimensional density profiles of water in contact with a solute of arbitrary shape: A RISM approach. *Chem. Phys. Lett.* **290**, 237–244 (1998).
58. F. Mrugalla, S. M. Kast, Designing molecular complexes using free-energy derivatives from liquid-state integral equation theory. *J. Phys.: Condens. Matter* **28**, 344004 (2016).
59. C. Trapnell, L. Pachter, S. L. Salzberg, TopHat: Discovering splice junctions with RNA-Seq. *Bioinformatics* **25**, 1105–1111 (2009).
60. M. Lawrence, W. Huber, H. Pagès, P. Aboyoun, M. Carlson, R. Gentleman, M. T. Morgan, V. J. Carey, A. Prlic, Software for computing and annotating genomic ranges. *PLOS Comput. Biol.* **9**, e1003118 (2013).
61. M. I. Love, W. Huber, S. Anders, Moderated estimation of fold change and dispersion for RNA-seq data with DESeq2. *Genome Biol.* **15**, 550 (2014).
62. A. Liberzon, C. Birger, H. Thorvaldsdóttir, M. Ghandi, J. P. Mesirov, P. Tamayo, The Molecular Signatures Database (MSigDB) hallmark gene set collection. *Cell Syst.* **1**, 417–425 (2015).
63. V. K. Mootha, C. M. Lindgren, K.-F. Eriksson, A. Subramanian, S. Sihag, J. Lehár, P. Puigserver, E. Carlsson, M. Ridderstråle, E. Laurila, N. Houstis, M. J. Daly, N. Patterson, J. P. Mesirov, T. R. Golub, P. Tamayo, B. Spiegelman, E. S. Lander, J. N. Hirschhorn, D. Altshuler, L. C. Groop, PGC-1α-responsive genes involved in oxidative phosphorylation are coordinately downregulated in human diabetes. *Nat. Genet.* **34**, 267–273 (2003).
64. M. W. Karaman, S. Herrgard, D. K. Treiber, P. Gallant, C. E. Atteridge, B. T. Campbell, K. W. Chan, P. Ciceri, M. I. Davis, P. T. Edeen, R. Faraoni, M. Floyd, J. P. Hunt, D. J. Lockhart, Z. V. Milanov, M. J. Morrison, G. Pallares, H. K. Patel, S. Pritchard, L. M. Wodicka, P. P. Zarrinkar, A quantitative analysis of kinase inhibitor selectivity. *Nat. Biotechnol.* **26**, 127–132 (2008).
65. M. I. Davis, J. P. Hunt, S. Herrgard, P. Ciceri, L. M. Wodicka, G. Pallares, M. Hocker, D. K. Treiber, P. P. Zarrinkar, Comprehensive analysis of kinase inhibitor selectivity. *Nat. Biotechnol.* **29**, 1046–1051 (2011).
66. A. E. Drilon, C. S. Sima, R. Somwar, R. Smith, M. S. Ginsberg, G. J. Riely, C. M. Rudin, M. Ladanyi, M. G. Kris, N. A. Rizvi, Phase II study of cabozantinib for patients with advanced *RET*-rearranged lung cancers, paper presented at 2015 ASCO Annual Meeting (2015).

Acknowledgments: We thank T. Zillinger from the University Hospital Bonn for sharing the Cas9 expression and the backbone of the pLenti-IRES-blasticidine vector system, F. Malchers and members of the Sos Lab and Thomas Lab for the technical support, A. Florin and U. Rommerscheidt-Fuß for supporting us with IHC staining, and P. Kibies and L. Eberlein as well as L. Goeminne and L. Clement for supporting the computational modeling. We thank W. Pao and N. von Bubnoff for the TPC-1 and Ba/F3 cell line. We thank AstraZeneca for supporting vandetanib for off-label use, SOBI for providing cabozantinib for compassionate use, and F. Aebersold and A. Hirschmann for the diagnostic work. We also thank A. Dar and R. Cagan for helpful discussions. **Funding:** This work was supported by the German federal state North Rhine Westphalia and by the European Union (European Regional Development Fund: Investing In Your Future) as part of the PerMed.NRW initiative (grant 005-1111-0025 to R.K.T., J.W., and R.B.) as well as the EFRE initiative (grant LS-1-1-030 to R.B., J.W., R.K.T., and M.L.S) and by the German Ministry of Science and Education (BMBF) as part of the e:Med program [grant nos. 01ZX1303 (to M.P.), 01ZX1603 (to R.K.T., J.W., and R.B.), and 01ZX1406 (to M.P. and M.L.S.)], by the Deutsche Forschungsgemeinschaft [through TH1386/3-1 (to R.K.T. and M.L.S. and KA1381/5-1 to (S.M.K.)], and by the German Consortium for Translational Cancer Research (DKTK) Joint Funding program. V.T. is the recipient of a joint European Respiratory Society/European Molecular Biology Organization Long-Term Research fellowship no. LTRF 2014-2951. N.Q.M. acknowledges that this work was supported by the Francis Crick Institute, which receives its core funding from Cancer Research UK (FC001115), the UK Medical Research Council (FC001115), and the Wellcome Trust (FC001115); by the NCI/NIH (grant reference 5R01CA197178); and by the Association for Multiple Endocrine Neoplasia Disorders MTC Research Fund. The authors acknowledge financial support by the Ministerium für Innovation, Wissenschaft und Forschung des Landes Nordrhein-Westfalen, the Senatsverwaltung für Wirtschaft, Technologie und Forschung des Landes Berlin, and the Bundesministerium für Bildung und Forschung (to O.P. and R.P.Z.). **Author contributions:** D.P., M.R., J.B., M.A.D., C.L., and D.S. performed the cloning and cell culture experiments. V.T., A.H.S., and R.B. analyzed the IHC and FISH images. Y.S. was responsible for the PDX establishment and measurements. J.S., F.M., Y.A., and S.M.K. performed the computational modeling. O.P. and R.P.Z. performed the quantitative phosphoproteomics and data analysis. M.K., M.B., A.R., J.S., J.E., M.A., and K.G. performed the in vitro kinase experiments and analyses. R.C., P.P.K., and N.Q.M. purified the recombinant RET fusion proteins and performed the thermal shift analyses. J.D., G.P., and O.G. contributed to the clinical patient data. F.L. and J.M.H. were responsible for the next-generation sequencing of RET. J.B. and M.P. analyzed the RNA-seq data. K.M.S. provided the compounds. D.P., M.R., J.B., M.D., F.L., J.W., N.Q.M., K.M.S., R.K.T., and M.L.S. interpreted the data and performed the statistical analyses. D.P., M.R., S.M.K., R.K.T., O.G., and M.L.S. wrote the manuscript. **Competing interests:** R.K.T. is a founder and consultant of NEO New Oncology GmbH and received commercial research grants from AstraZeneca, EOS, and Merck KgaA and honoraria from AstraZeneca, Bayer, NEO New Oncology AG, Boehringer Ingelheim, Clovis Oncology, Daiichi-Sankyo, Eli Lilly, Johnson & Johnson, Merck KgaA, MSD, Puma, Roche, and

Sanofi. F.L. and J.M.H. are employees of NEO New Oncology GmbH. M.L.S received commercial research grants from Novartis. K.M.S and M.L.S. are both patent holders for the compound AD80. K.M.S. and M.L.S., together with A. C. Dar, T. K. Das, T. G. Bivona, and R. L. Cagan, are inventors on a patent application (applicants Mount Sinai School of Medicine and the Regents of the University of California; publication no. US 2014/0243357 A1) that covers the compounds AD80, AD57, and AD81 and the use thereof. All other authors declare that they have no competing interests. **Data and materials availability:** RNA-seq data were deposited at the European Genome-phenome Archive (www.ebi.ac.uk/ega/; accession number EGAS00001002335). The mass spectrometry proteomics data have been deposited to the ProteomeXchange Consortium via the PRIDE (Proteomics Identifications) partner repository with the data set identifier PXD006006. The Shokat Lab provided AD80, AD81, and AD57; compounds will be made available upon request. The remaining compounds were purchased from LC Laboratories and Selleckchem.

Submitted 21 July 2016
Resubmitted 3 February 2017
Accepted 21 March 2017
Published 14 June 2017
10.1126/scitranslmed.aah6144

Citation: D. Plenker, M. Riedel, J. Brägelmann, M. A. Dammert, R. Chauhan, P. P. Knowles, C. Lorenz, M. Keul, M. Bührmann, O. Pagel, V. Tischler, A. H. Scheel, D. Schütte, Y. Song, J. Stark, F. Mrugalla, Y. Alber, A. Richters, J. Engel, F. Leenders, J. M. Heuckmann, J. Wolf, J. Diebold, G. Pall, M. Peifer, M. Aerts, K. Gevaert, R. P. Zahedi, R. Buettner, K. M. Shokat, N. Q. McDonald, S. M. Kast, O. Gautschi, R. K. Thomas, M. L. Sos, Drugging the catalytically inactive state of RET kinase in RET-rearranged tumors. *Sci. Transl. Med.* **9**, eaah6144 (2017).

Science Translational Medicine

Drugging the catalytically inactive state of RET kinase in RET-rearranged tumors

Dennis Plenker, Maximilian Riedel, Johannes Brägelmann, Marcel A. Dammert, Rakhee Chauhan, Phillip P. Knowles, Carina Lorenz, Marina Keul, Mike Bührmann, Oliver Pagel, Verena Tischler, Andreas H. Scheel, Daniel Schütte, Yanrui Song, Justina Stark, Florian Mrugalla, Yannic Alber, André Richters, Julian Engel, Frauke Leenders, Johannes M. Heuckmann, Jürgen Wolf, Joachim Diebold, Georg Pall, Martin Peifer, Maarten Aerts, Kris Gevaert, René P. Zahedi, Reinhard Buettner, Kevan M. Shokat, Neil Q. McDonald, Stefan M. Kast, Oliver Gautschi, Roman K. Thomas and Martin L. Sos

Sci Transl Med **9**, eaah6144.
DOI: 10.1126/scitranslmed.aah6144

RET-ting out lung tumors

Gene fusions and rearrangements serve as oncogenic drivers in a number of tumor types, and some of these can be targeted with existing drugs. *RET* rearrangements have been identified as drivers in some lung adenocarcinomas, but previous attempts to target RET have not been successful. Plenker *et al*. determined why the drugs previously proposed for inhibiting RET were not sufficiently potent and showed that successful inhibition of RET requires the ability to bind RET in its catalytically inactive conformation, known as the "DFG-out conformation," thus locking it in an inactive state. The authors also identified drugs that bind RET in the desired conformation and demonstrated their efficacy in patient-derived xenograft models.